Accurate Discretization of Vertically-Averaged Models of CO2 Plume Migration

Knut-Andreas Lie Ingeborg Skjelkvåle Ligaarden Halvor Møll Nilsen

July 15, 2010

Abstract

When CO_2 is injected into a deep formation, it will migrate as a plume that moves progressively higher in the formation, displacing the resident brine. The invasion front is driven by gravity, and the upward movement of the plume is limited by a low-permeable caprock. Several authors have recently proposed to make a sharp-interface assumption and only describe the plume migration in a vertically-averaged sense. For inhomogeneous permeability, the plume migration is then described by a system of conservation laws with spatially discontinuous flux. If one disregards dissolution and residual trapping, the system reduces to a scalar conservation law with a spatially dependent flux function, which may exhibit different solutions depending on the entropy condition that is enforced to pick a unique solution. We propose a certain set of assumptions that lead to the so-called minimum-jump condition and derive the corresponding solutions to the Riemann problem. Solutions to this problem are fundamental when developing accurate Godunov-type schemes. Here, we take a slightly different approach and present an unconditionally stable front-tracking method, which is optimal for this type of problem. Moreover, we verify the well-known observation that a standard upstream mobility discretization can give wrong solutions in certain cases.

Introduction

When CO_2 is injected into a deep formation, such as a saline aquifer or an abandoned petroleum reservoir, it will spread out from the injection well and displace the resident brine. At relevant conditions, the CO_2 is in a supercritical state and will form a second liquid phase that is slightly soluble in water, but also less dense and much less viscous than the resident brine. The injected CO_2 will therefore migrate as a plume that moves radially outwards and progressively higher in the formation, limited above by the low-permeable caprock that bounds the aquifer or reservoir. Although the invasion front is mainly driven by gravity, there are several other important processes going on, like dissolution of CO_2 into brine, formation of wet CO_2 because of evaporation of water into the CO_2 phase, formation of a front of dry CO_2, precipitation of salt, etc. Likewise, the time scale of interest for a CO_2 storage operation will typically be hundreds or thousands of years, during which the plume may move several tens of kilometres. On the other hand, the CO_2 plume will tend to form a very thin fringe under the rock. Complex physics, long time scale, and large differences in the lateral and vertical scales pose severe challenges to the numerical methods used to model CO_2 migration. In particular, several benchmark studies, see e.g., Class et al. (2009), have shown that it is difficult to obtain 3D simulations with sufficient vertical resolution.

Vertical equilibrium (VE) models have long traditions for describing flow in porous media. In hydrology, the assumption of vertical equilibrium is known as the Dupuit approximation and is a good description of nature for most flow situations. In the oil industry, VE models were extended to two-phase and three-phase segregated flow (Martin, 1958; Coats et al., 1967; Martin, 1968). In particular, Coats et al. (1971) advocated comparing simulations of 2D vertical cross-sections to corresponding 1D simulations with a vertical averaged model to check if the assumptions for the latter was present, and then use this model to save computational time or gain resolution whenever applicable. As computational resources increased, VE models became less and less used. Recently, however, there has been a renewed interest (Nordbotten et al., 2005; Celia et al., 2006; Nordbotten and Celia, 2006) in these methods as a means to simulate large-scale CO_2 migration, for which a sharp-interface assumption with vertical equilibrium may be reasonable because of the large density and viscosity differences between supercritical CO_2 and brine. Because the time scales of interest are long and the injection volumes are large, the assumptions of the VE models are fulfilled for large space and time domains. Indeed, in many cases the errors resulting from the VE assumption may be significantly less that the errors introduced by the overly coarse resolution needed to make 3D simulation model computationally tractable. Vertically averaged (VA) simulations may then be attractive to increase (lateral) resolution while saving computational cost.

The VE formulation for multiphase flow in heterogeneous media leads to a system of a pressure and a transport equation that can be written in a standard fractional-flow formulation. Many authors (Hesse et al., 2007, 2008; MacMinn and Juanes, 2009; Huppert and Woods, 1995; Lyle et al., 2005; Vella and Huppert, 1995) have considered gravity-driven flow in the VA equations in detail for *homogeneous* permeability. In particular, Ruben Juanes and Szulczewski (2010) derived analytical solutions based on Riemann problems in the hyperbolic limit (lateral scale $\gg$ vertical scale). Analytical and numerical results from VA calculations can be used to provide order-of-magnitude estimates for travel times and distances on basin scale and enable simplified calculations of the CO_2 inventor. Likewise, simplified VA calculations are well suited in combination with Monte–Carlo simulations to calculate stochastic leakage estimates for scenarios with large uncertainty.

For *heterogeneous* media, the pseudo relative-permeability curves appearing in the VA transport equation include the vertical variation of the horizontal permeability (Coats et al., 1971; Nordbotten and Celia, 2010). This introduces a hyperbolic term with a discontinuous flux function in the transport equations. Analytical solutions for hyperbolic equations with discontinuous flux functions are significantly more complex to derive, in particular, for equations with nonmontone flux functions as in the VA models. The study of accurate and consistent numerical methods for equations with discontinuous flux functions has been given much attention in recent years (Andreianov et al., 2010; Burger et al., 2009; Adimurthi

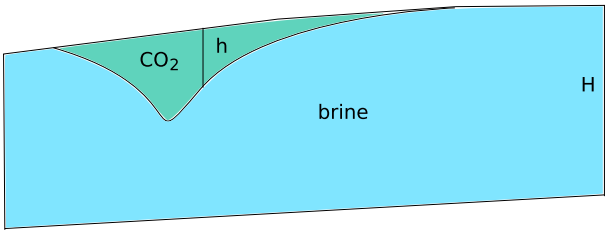

Figure 1 *Illustration of the CO_2 plume as assumed in the VA modelling.*

et al., 2005). In particular, Mishara and Jaffré (2010) showed that the standard upstream mobility discretization will give non-physical solutions for two-phase transport models with changing rock type. In a recent paper, Andreianov et al. (2010) pointed out that there is a continuum of different entropy solutions to hyperbolic equations with discontinuous flux functions. They also constructed a numerical method that will converge to each of the different entropy solutions, depending on a parameter at the flux discontinuities. Herein, we investigate the appropriate interface conditions for the scalar VA model derived by neglecting dissolution and residual trapping, and solve the Riemann problem associated with the most relevant shapes of the flux functions. Based on these solutions, we construct an unconditionally stable front-tracking method. We show that this method is capable of resolving the dynamics of the model in the hyperbolic limit. For injection and long-time storage of large amounts of CO_2, it is crucial to have a method that can give accurate results on the large scale corresponding to the hyperbolic limit. Finally, based on our Riemann solutions we point out the particular cases in which a standard upstream mobility discretization will fail.

Mathematical Formulation

In the following, we will use VA transport equations written on the following form

$$\frac{\partial s}{\partial t} + \frac{\partial}{\partial x}\Big[f(s,x)v + f_g(s,x)\big[g(x) + \nabla p_c(s,x)\big]\Big] = q(x). \tag{1}$$

Referring to Figure 1, $s = h/H$ is the relative height of the CO_2 plume and is a function of time t and the spatial distance x along the dipping reservoir. The function g is the gravity component along x, v is the drift in the aquifer (which we for simplicity assume to be known), q is a source term, f is the fractional flow function, and f_g the gravitational fractional flow. The latter two are given by

$$\lambda_{co_2}(s,x) = \int_0^{sH(x)} k_{co_2}(1)K_x(z,x)dz, \qquad \lambda_w(s,x) = \int_{sH(x)}^{H(x)} k_w(1)K_x(z,x)dz$$

$$f(s,x) = \frac{\lambda_{co_2}(s,x)}{\lambda_{co_2}(s,x) + \lambda_w(s,x)}, \qquad f_g(s,x) = \lambda_w(s,x)f(s,x),$$

where k_α denote the relative permeabilities of brine and CO_2; to simplify our argument, both viscosities are assumed to be equal unit. If we disregard capillary forces in the underlying flow model, our VA-equivalent of the capillary term reads $p_c(s,x) = g\Delta\rho\, s$. A thorough derivation of similar VA models can be found in e.g., (Coats et al., 1967; Nordbotten and Celia, 2010).

Having established our model, we point out a few qualitative features: For constant x, the flux function $f(s,x)$ is monotone whereas $f_g(s,x)$ has one critical point and $f_g(0,x) = f_g(1,x) = 0$. Moreover, $\partial_s p_c < 0$ because $g\Delta\rho$ is negative. To illuminate the relative importance of the various terms, we change variables and let $x \to xL$, where x now is a dimensionless distance. Then the VA transport equation (1) takes the form

$$\frac{\partial s}{\partial t} + \frac{1}{L}\frac{\partial}{\partial x}\left(f(s,x)v + Hf_g(s,x)\big[g(x) + \frac{H}{L}\nabla p_c(s,x)\big]\right) = q(x), \tag{2}$$

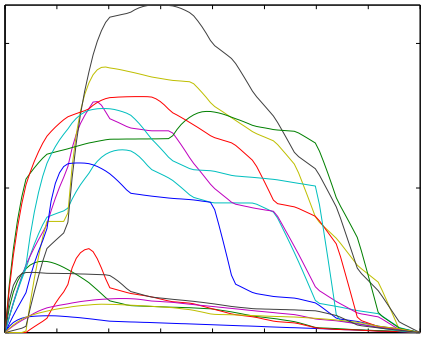

Figure 2 *Illustration of the function $h(s,\cdot)$ sampled at different locations in a realistic reservoir model.*

from which it is clear that the large-scale ($H/L \gg 1$) and the hyperbolic limits are the same if all functions vary smoothly on scales less then the large scale. Moreover, writing the equation in this form also highlights the importance of using a stable discretisation for the hyperbolic part since the parabolic term is degenerate at the endpoint. Hence, for some value of s, the numerical dispersion will dominate the physical dispersion arising from the ∇p_c term. The importance for considering the degenerate points of the parabolic term when choosing a numerical method for a mixed hyperbolic–parabolic equation has been studied by many authors. The interested reader may consult Holden et al. (2010) for an overview of relevant references.

In the rest of the paper, we will focus entirely on the large-scale limit, in which case (1) becomes a hyperbolic conservation law. To simplify the presentation, we assume no drift in the aquifer, giving the discontinuous flux problem

$$\frac{\partial s}{\partial t} + \frac{\partial}{\partial x} h(s,x) = q(x), \qquad h(s,x) = f_g(s,x)g(x), \tag{3}$$

for which the solution must be found in a weak sense. Weak solutions of are not unique and an entropy condition must be imposed to single out the unique physically correct solution. If $h(\cdot,x)$ is a *continuous* function, the correct entropy solution can be found from the standard vanishing-viscosity method; that is, we add the term εs_{xx} to the right-hand side of (3) and select our physically correct solution $s(x,t)$ as the limit of $s^\varepsilon(x,t)$ as $\varepsilon \to 0$, giving the classical Kruzkov framework for entropy conditions (Kružkov, 1970). When $h(\cdot,x)$ is a *discontinuous* function, (3) may possess many different L^1-contractive semigroups of solutions that correspond to different physical phenomena modelled by the same equation, but with different dissipative processes occuring on the discontinuities of the solutions (Andreianov et al., 2010). To derive entropy conditions that are suitable for (3), we will therefore in the next section study the underlying physical phenomenon giving rise to the discontinuous behaviour in the VA model. Knowledge of what are the appropriate entropy conditions is important when developing numerical schemes that are guaranteed to capture the large-scale effects of unresolved subscale phenomena correctly.

Numerical Investigation of the Discontinuous Riemann Problem

The spatial dependence in the flux function of (3) comes from two different effects: (i) topographical variations of the top and bottom surfaces bounding the aquifer, and (ii) spatial dependence in the permeability. Herein, we will neglect the former and focus on the behaviour of the permeability $K(x,z)$ as a function of x. Figure 2 shows a set of flux functions sampled from a realistic reservoir model that has relatively small permeability variations.

To develop an understanding of what effects a permeability-induced discontinuity will have on the solutions to (3), we assume that although $h(s,x)$ will appear as discontinuous on the large scale, there is a smaller scale on which the variation in $k(x,z)$ will give a function $h(\cdot,x)$ that is continuous in x. On

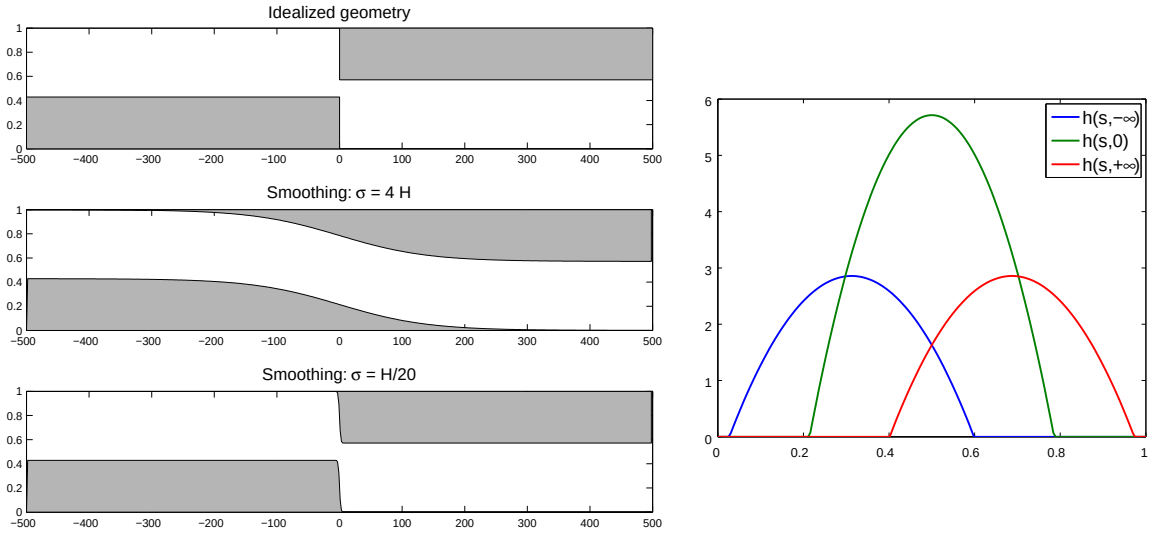

Figure 3 *The left columns shows the idealised aquifer geometry with impermeable regions shown in grey. The top plot shows the geometry that gives a discontinuous flux, whereas in the lower plots the impermeable steps have been smoothed so that the flux function $h(\cdot, x)$ becomes continuous in x. The right plot shows the corresponding flux function.*

this much smaller scale, the transport equation (3) will not have a discontinuous flux, and the physically correct solution will be the one predicted using the standard Kruzkov entropy theory (Kružkov, 1970). The assumption of the existence of such a scale is, of course, a simplification, but we believe that it is reasonable for our purpose herein.

Specifically, we will consider the behaviour of a highly idealised case where the aquifer is rectangular and contains two impermeable steps as illustrated in Figure 3. This particular setup will exaggerate effects observed in realistic models with finite permeability variations. In our set up, $h(x, s)$ is designed such that

$$\lim_{x \to \pm\infty} h(s, x) = h^{\pm}(s). \tag{4}$$

To resolve the small-scale behaviour using the standard Kruzkov theory, we smooth the edges of the impermeable regions so that the flux function will change smoothly on a length scale σ. That is, we set

$$h(s,x) = (h^+(s)h_\sigma(x) + h^-(s)\big(1 - h_\sigma(x)\big))(1 + exp(x/\sigma)), \qquad h_\sigma(x) = \tfrac{1}{2}\big(1 - \tanh(\tfrac{x}{\sigma})\big) \tag{5}$$

Figure 3 shows the geometries for two different choices of the length scale σ as well as the resulting flux functions.

As we stated above, our interest will eventually be in the effects that this permeability heterogeneity has on the flow on a much larger scale. On the large scale, the interface conditions will be given by

$$\lim_{x \to \pm\infty} s = s^{\pm}, \tag{6}$$

which has to fulfil the Rankine–Hugoniot condition $f^-(s^-) = f^+(s^+)$. To determine the interface states, we start the simulations with initial condition

$$s(x,0) = \begin{cases} s_L, & \text{for } x < 0, \\ s_R, & \text{otherwise.} \end{cases} \tag{7}$$

and solve to stationary state. For a given fine-scale flux $f(s, x)$, this gives a unique mapping from (s^L, s^R) to (s^-, s^+). The discontinuous flux problem, on the other hand, does not give such a unique

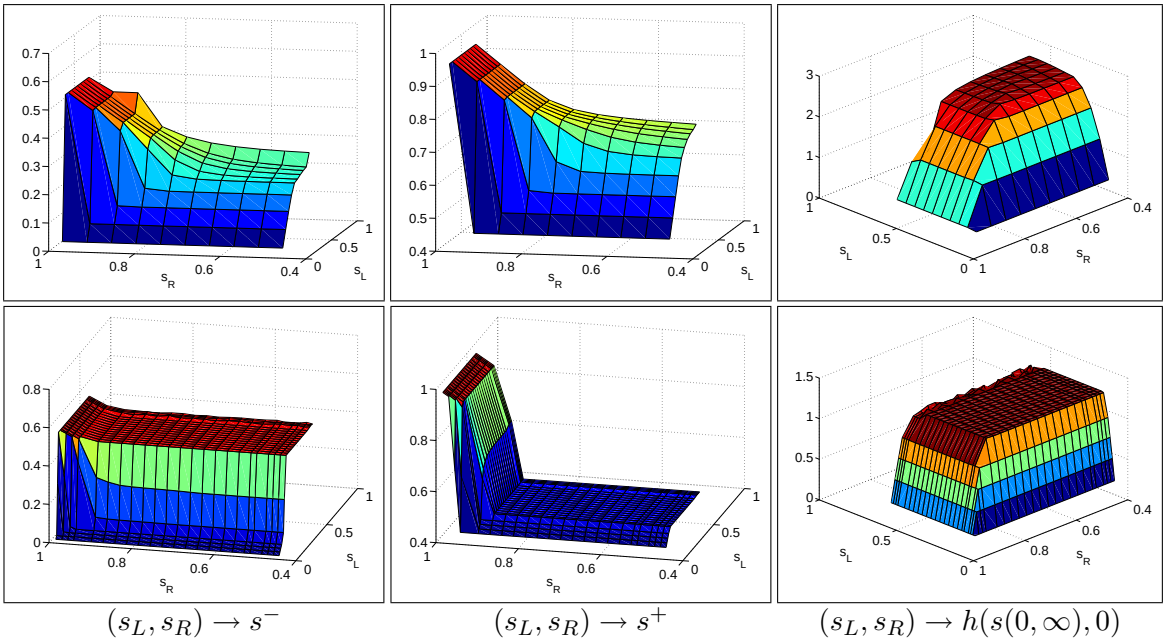

Figure 4 *Numerical calculation of the Riemann problem corresponding to Figure 3 for $\sigma = 4H$ (top row) and $\sigma = H/20$ (bottom row).*

relationship, and when choosing a numerical method for the large-scale problem we should ensure that it picks out the unique mapping that reflects the correct fine-scale behaviour.

A careful computational analysis of our setup suggests that the correct entropy condition on the large scale is the so-called minimal jump condition, which selects the weak solution that has the least jump across the stationary interface where the flux function is discontinuous. To support this conclusion, we present simulations of two opposite cases of the flux function given above, (5), corresponding to $\sigma = 4H$ and $\sigma = H/20$. Figure 4 shows the resulting mappings for these two cases. To help the reader understand the figure, we consider the solution of the corresponding large-scale Riemann problem:

$$\frac{\partial s}{\partial t} + \frac{\partial h(s,x)}{\partial x} = 0, \qquad (s,h) = \begin{cases} (s_L, h^-(s)), & \text{for } x < 0, \\ (s_R, h^+(s)), & \text{otherwise.} \end{cases} \tag{8}$$

We rescale the problem slightly so that $0 \le h(s,x) < 1$, fix $s_R = 0.44$, and consider how the Riemann solution satisfying the minimal-jump condition changes with varying values of s_L. In Figure 5, we have plotted the Riemann solution in (s,h) and (x,s) space. Letting s_L vary in the interval $[0, 0.475]$, we observe three different types of Riemann solutions (in the following $\bar{s}$ will denote the value at which $h^-(s) = h^+(s)$):

Region 1 For $s_L \subset [0, 0.04]$, we have that $h^-(s_L) < h^+(s_r)$ and the solution consists of a stationary shock at $x = 0$ between the values s_L and $s^- = s_L + 0.4$ and a shock between the values s^- and s_R that propagates to the right.

Region 2 For $s_L \subset [0.04, 0.1]$, the solution consists of a stationary shock at $x = 0$ between the values s_L and $s^- = s_L + 0.4$ and a rarefaction wave between the values s^- and s_R that propagates to the right.

Region 3 For $s_L \subset [0, 0.04]$ the solution consists of a shock between values s_L and $s^- = \bar{s} = 0.5$ that propagates leftward and a rarefaction fan between values s_R and $\bar{s}$ that propagates to the right.

In Regions 1 and 2, the interface value s^- is continuously increasing, as is also observed in Figure 4. The interface value $\bar{s}$ observed in Region 3 in Figure 5 clearly corresponds to the plateaus formed in the

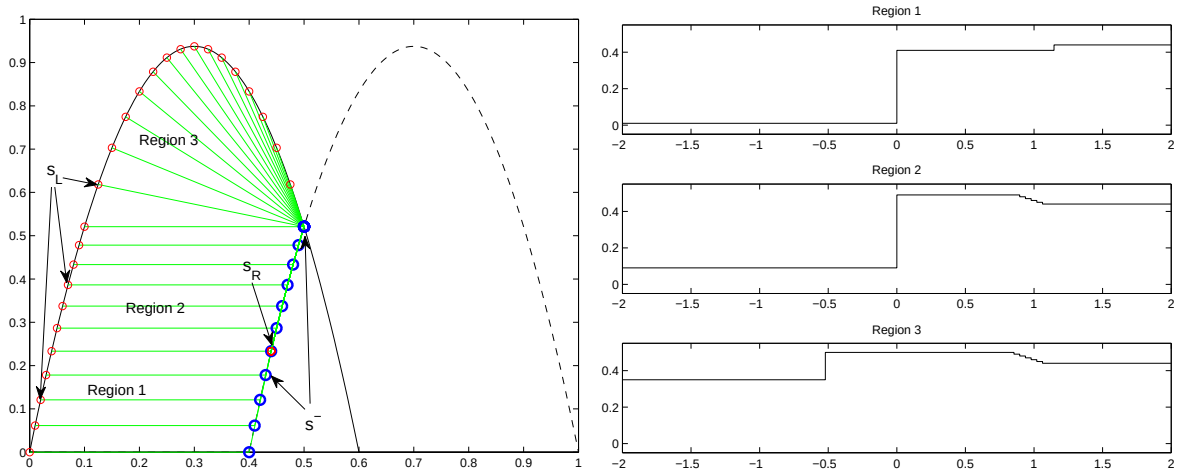

Figure 5 *Solution to the large-scale Riemann problem* (8) *for fixed* $u_R = 0.44$*. The left plot shows the solutions in* (s, f) *space, where the red circles are the left states that increase in the interval* $[0, 0.475]$*, the blue circles are the left states at* $s^- = s(0^-, t)$*, and the green lines represents the shocks (and rarefactions) in the Riemann fan. The plots in the right column show the similarity solutions* $s(x, t) = s(x(t)$ *in the three different regions.*

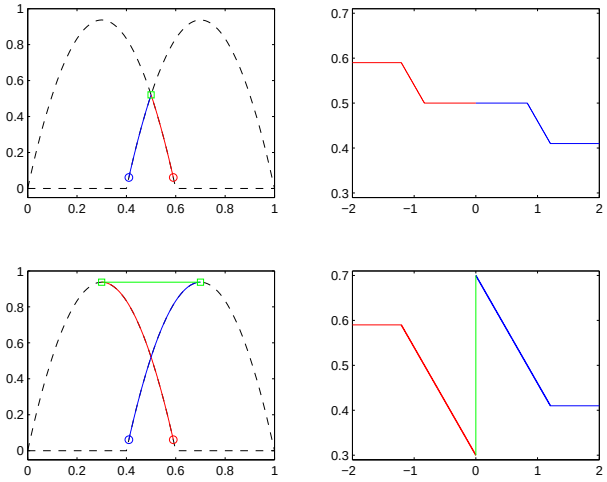

Figure 6 *Comparison of the Riemann solution for* $s_L = 0.59$ *and* $s_R = 0.41$ *obtained with the minimal-jump condition (top) and the Mishra–Jaffré condition (bottom). States to the left of the interface are in red colour, states to the right are in blue, and states at the interface are in green.*

s^- and s^+ surfaces for $\sigma = H/20$ in Figure 4. In summary, we believe that these results confirm that the minimal-jump condition is correct when considering large-scale behaviour.

For the opposite case of $\sigma = 4H$, we see that the plateau values are significantly smaller for s^- and significantly larger for s^+ and that the interface flux is also much higher. These solutions seem to correspond to the admissibility condition advocated by Mishara and Jaffré (2010), which may be correct when studying flows where the transitions in $K(x, z)$ do not occur on a scale that is significantly smaller. It may be illuminating to contrast Riemann solutions obtained with the minimal-jump and the Mishra–Jaffré condition. This is done in Figure 6 for a specific set of initial conditions. Both solutions predict two rarefaction fans emanating from $x = 0$, but whereas the Mishra–Jaffré solution has a stationary discontinuity and introduces values outside the span of the initial states, the minimal-jump solution is monotone and has no stationary discontinuity at $x = 0$. These results confirm the observations in Figure 4: the flux at the interface is significantly higher for the Mishra–Jaffré solution than for the minimal-jump solution, and the interface states observed in Figure 6 seem to correspond to the plateau values in Figure 4.

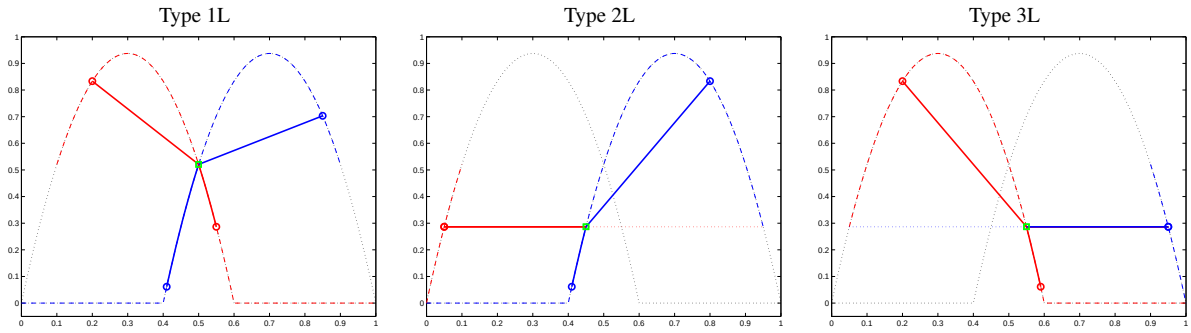

Figure 7 *Solution to the Riemann problem for the conceptual setup shown in Figure 3. The red/blue circles denote the left/right states, the solid red/blue lines denote waves moving to the left/right, the dashed red/blue lines show all the left/right states that fall into the same category of solutions, and the green circle shows the new intermediate state introduced at $x = 0$. If the solid lines coincide with the underlying flux function, the corresponding wave is a rarefaction, and otherwise it is a shock.*

The observations above have also been partially confirmed by a large number of 2D simulations of the full two-phase equations on setups where we instead of the impermeable regions in Figure 3 used low-permeable regions. However, here it has been difficult to obtain results with sufficient resolution to produce a plot similar to Figure 4.

Solution to the Riemann Problem

In the previous section, we considered a simplified and conceptual model of a permeability-induced discontinuity in the large-scale VA transport equation (3). By studying the same problem on a much smaller scale, on which the flux discontinuity is replaced by a smooth transition, we derived an appropriate admissibility condition that will enable us to pick the unique entropy-weak solution of (3). In this section, we will continue with the idealised model from the previous section and use the entropy to derive the full solution to the Riemann problem (8). Solutions to the Riemann problem are fundamental when using the Godunov approach for developing accurate (high-resolution) schemes. We emphasise that although our conceptual model is very simple, it contains (almost all) the characteristics necessary to develop Riemann solutions for flux functions arising in realistic injection scenarios. Indeed, the only purpose of exaggerating the permeability contrasts is to make the presentation of Riemann solutions more transparent to the reader.

Figure 7 shows all permissible solutions to the Riemann problem for the setup in Figure 3. The solutions can be divided into three different categories:

Type 1L If the left state fulfils either $s_L \geq \bar{s}$ or $h^-(s_L) \geq h^-(\bar{s})$ and the right state fulfils either $s_R \leq \bar{s}$ or $h^+(s_R) \geq h^+(\bar{s})$, then the solution will consist of two ordinary Riemann fans. The first Riemann problem is defined between s_L and $\bar{s}$ using the flux $h^-(s)$ and gives waves with negative speeds that propagate leftward from $x = 0$; the wave will be a shock if $s_L < \bar{s}$ and a rarefaction if $s_L > \bar{s}$ (states with $s_L > 0.6$ correspond to CO_2 in the impermeable region and are therefore not interesting here). Likewise, the second Riemann problem is defined between s_R and $\bar{s}$ using the flux $h^+(s)$ and gives waves with positive speeds that propagate rightward from $x = 0$; the wave will be a rarefaction if $s_R < \bar{s}$ and a shock if $s_R > \bar{s}$.

Type 2L If $s_L < \bar{s}$ and $h^-(s_L) < h^-(\bar{s})$, and either $s_R < \bar{s}$ or $h^+(s_R) \geq h^-(s_L)$, the solution will consist of: (i) a stationary shock at $x = 0$ between the values s_L and the value s^+ that fulfils the conditions $h^+(s^+) = h^-(s_L)$ and $\frac{dh^+}{dx}(s^+) > 0$, and (ii) a Riemann fan with positive wave speeds defined as the solution of the ordinary Riemann problem between s_R and s^+.

Type 3L If $s_R > \bar{s}$ and $h^+(s_R) < h^+(\bar{s})$, and either $s_L < \bar{s}$ or $h^-(s_L) \geq h^+(s_R)$, the solution will consist of: (i) a stationary shock at $x = 0$ between the values s_R and the value s^- that fulfils

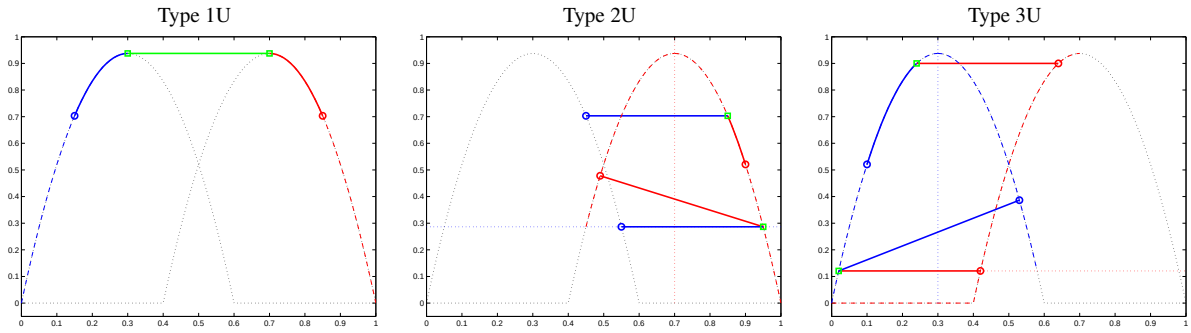

Figure 8 *Solution to the Riemann problem for the conceptual setup opposite to the one shown in Figure 3. The colours and symbols are explained in Figure 7.*

the conditions $h^-(s^-) = h^+(s_R)$ and $\frac{dh^-}{dx}(s^-) < 0$, and (ii) a single Riemann fan with negative wave speeds defined as the solution of the ordinary Riemann problem between s_L and s^-.

For completeness, we also present the solution for the opposite case of Figure 3 in which the impermeable region is at the top left of the discontinuity line and at the bottom right of the line. Figure 8 shows the three different categories of Riemann solutions:

Type 1U Let $a^\pm = \operatorname{argmax} h^\pm(s)$. Then if $s_L \geq a^+$ and $s_R \leq a^-$, the solution consists of: (i) a rarefaction wave with negative speeds connecting the states s_L and a^-, (ii) a stationary shock connecting a^- and a^+, and (ii) a rarefaction wave with positive speeds connecting a^+ and s_R.

Type 2U If $s_R > a^+$ and either $s_L > a^-$ or $f^-(s_L) > f^+(s_R)$, the solution consists of: (i) a stationary shock connecting s_R to the value s^- that fulfils the conditions $h^-(s^-) = h^-(s_R)$ and $\frac{dh^-}{dx}(s^-) < 0$, and (ii) a rarefaction fan connecting s_L and s^- if $s_L > s^-$ or a shock between s_L and s^- otherwise.

Type 3U Symmetric to Type 2, with a stationary shock connecting s_L and s^+ and either a rarefaction wave or a shock connecting s^+ and s_R, depending upon whether $s_R < s^+$ or not.

In the next section we will use the solutions of the Riemann problem to develop a semi-analytical method that is particularly efficient for computing accurate approximations to (3).

An Unconditionally Stable Front-Tracking Method

The Riemann problems solved in the previous section take a particularly simple form if the flux function $h(s, \cdot)$ is a piecewise linear function of s. Then, all rarefaction fans will be self-similar step functions, i.e., consist of a set of constant states separated by straight space-time rays. If also $h(\cdot, x)$ and $s(x, 0)$ are piecewise constant functions of x, we can solve (3) *analytically* by solving the local Riemann problems posed by the initial data and keep track of all the resulting discontinuities (shocks and space-time rays in rarefaction waves) and solve new Riemann problems whenever two of them collide.

The algorithm is perhaps best illustrated by considering a problem. To this end, we consider the domain $[-2, 2]$, set $s(x, 0) \equiv 0.56$, and impose flux discontinuities at $x = \pm 0.5$ corresponding to three impermeable regions along the upper, lower, and upper boundaries of the aquifer. Figure 9 shows the resulting solution profiles and the corresponding discontinuities plotted in (x, t) space. The Riemann problem at $x = -0.5$ is of Type 2U, giving a discontinuity propagating to downward, corresponding to a CO_2 slug forming in front of the step. The Riemann problem at $x = 0.5$ is of Type 1L, giving a rarefaction wave propagating downward and a shock going up-slope. Just before $t = 0.2$, the tip of the rarefaction wave reaches the left discontinuity; this corresponds to brine flowing over the step and down under the increasing CO_2 slug in front of the step.

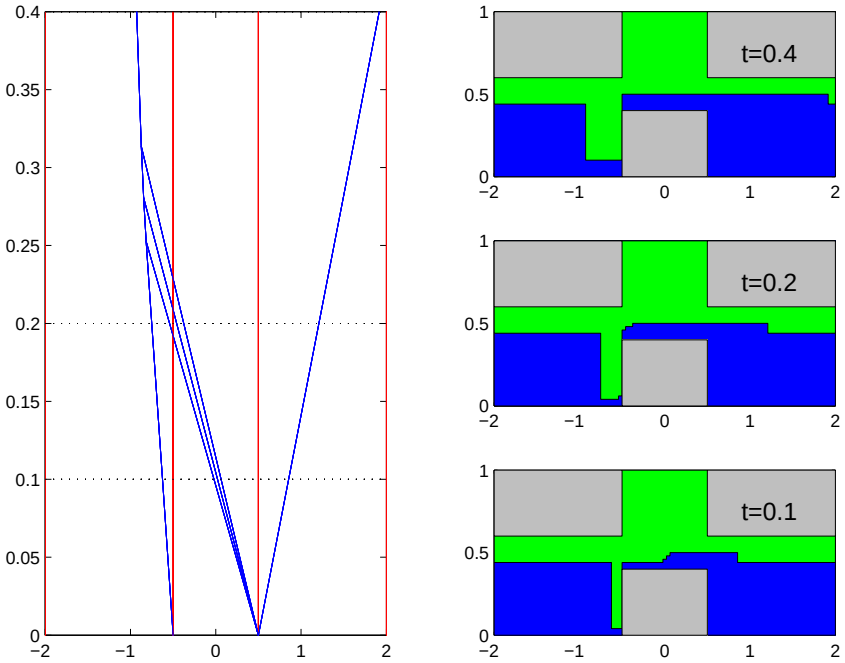

Figure 9 *Illustration of the front-tracking algorithm. The left plot shows the discontinuities in (x,t) space and the plots in the right column show the solutions at times $t = 0.1$, 0.2, and 0.4.*

For a general problem, one can make the piecewise constant/linear approximations to $s(x,0)$ and $h(s,x)$ and solve the corresponding *approximate* PDE problem analytically as an alternative to using a finite-volume or finite-element method. The resulting method is called *front tracking* and has been used previously by many authors to study flow in porous media. Although the method is admittedly more complex to implement than a standard finite-volume method, is has several nice properties. First of all, it is unconditionally stable, which is an advantage when studying long-time behaviour in large-scale domains. Moreover, it is grid-independent (apart from the approximation of $s(x,0)$ and $h(\cdot,x)$), and gives sharp resolution of shock fronts and other discontinuities. We refer readers interested in more details to the book by Holden and Risebro (2002).

Comparison with the Upstream Mobility Scheme

The upstream mobility scheme is widely used within hydrology and petroleum engineering, and will therefore typically be implemented in solvers used to study CO_2 storage. For the setup analysed herein, this finite-volume scheme takes a simple form:

$$s_i^{n+1} = s_i^n - \frac{\Delta t}{\Delta x}\Big[\frac{\lambda_{co_2}(s_i^n)\lambda_w(s_{i+1}^n)}{\lambda_{co_2}(s_i^n)+\lambda_w(s_{i+1}^n)} - \frac{\lambda_{co_2}(s_{i-1}^n)\lambda_w(s_i^n)}{\lambda_{co_2}(s_{i-1}^n)+\lambda_w(s_i^n)}\Big] \tag{9}$$

where s_i^n is the average height of the CO_2 plume in grid cell i at time $n\Delta t$.

In a recent publication, Mishara and Jaffré (2010) demonstrated that the upstream mobility scheme can produce wrong results for discontinuous flux problems modelling two-phase flow with relative permeability changing with the rock type. Here, we will verify that the method produces wrong solutions also for the large-scale VA transport equation (3). To this end, we revisit the Riemann problem from Figure 6, with $s_L = 0.59$ and $s_R = 0.41$. Figure 10 shows the solution computed by the upstream mobility scheme, which we recognise as the solution satisfying the Mishra–Jaffré admissibility condition, which our analysis has shown is *not* the physically correct solution. The figure also shows the solution of a Type 2L Riemann problem, for which our entropy solution would consist of a single shock propagating leftward.

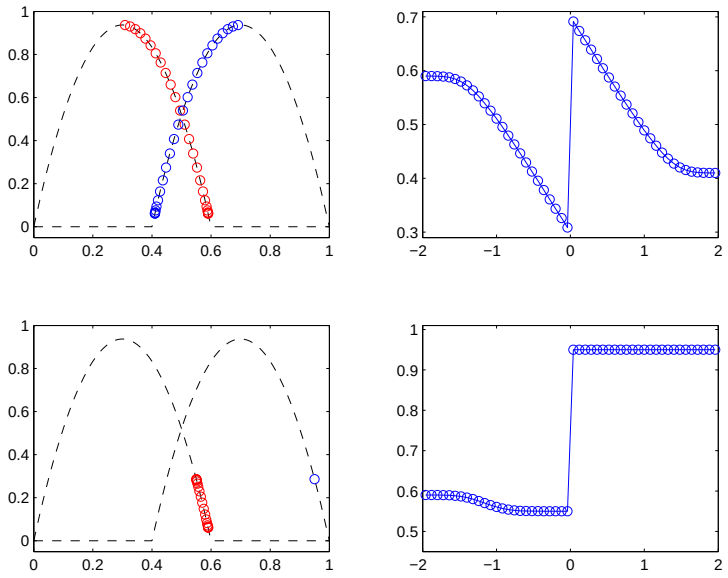

Figure 10 *Solution of Riemann problem of Type 1L with initial states* $s_L = 0.59$ *and* $s_R = 0.41$ *(top) and Type 2L with initial states* $s_L = 0.59$ *and* $s_R = 0.41$ *(bottom) computed with the upstream mobility scheme* (9).

Concluding Remarks

In this paper, we have considered scalar conservation laws with discontinuous flux arising from vertically-averaged models for CO_2 migration on large spatial and long temporal scales. Recent research has shown that discontinuous flux problems can have very different solutions depending on the physics they model. To derive the correct admissibility conditions, we considered an idealised flow problem on a much smaller scale than the scale of interest for migration studies. Our numerical experiments indicate that admissible solutions on the large scale should be selected using the so-called minimal jump condition; the determining factor here is how the continuous fine-scale flux functions approach their discontinuous large-scale limit. This is again determined by the fine-scale permeability behaviour. Other admissibility conditions are obtained if we make different assumptions. In this aspect, the minimal jump and the Mishra–Jaffré conditions appear as end-member cases.

Using the admissibility condition, we derived the full entropy solution of the Riemann problem. Riemann problems are fundamental in the design of high-performance numerical method. As an example of such a method, we briefly presented a semi-analytical front-tracking method that has previously shown to be near-optimal for 1D (scalar) conservation laws. Moreover, the method is a key ingredient in efficient operator splitting methods for 2D parabolic problems of the form (1) that have a strong hyperbolic character, see Holden et al. (2010). How to apply these methods to study large-scale CO_2 migration is still a topic for further research.

Finally, we verified an earlier observation by Mishara and Jaffré (2010) that the widely used upstream mobility scheme will produce incorrect solutions in several cases for (8). At the time of writing, it is not clear how important this is for practical computations of real-life models, but the issue should be looked into to increase the confidence in computations using vertically-averaged models.

References

Adimurthi, Mishra, S. and Gowda, G.D.V. [2005] Optimal entropy solutions for conservation laws with discontinuous flux function. *Journal of Hyperbolic Differential Equations*, **2**(4), 783–837.

Andreianov, B., Karlsen, K.H. and Risebro, N.H. [2010] A theory of L^1-dissipative solvers for scalar conservation laws with discontinuous flux. *submitted*.

Burger, R., Karlsen, K.H. and Towers, J.D. [2009] An Engquist-Osher-type scheme for conservation laws with discontinuous flux adapted to flux connections. *SIAM J. Numer. Anal.*, **47**(3), 1684–1712.

Celia, M.A., Bachu, S., Nordbotten, J.M., Kavetski, D. and Gasda, S. [2006] A risk assessment tool to quantify CO_2 leakage potential through wells in mature sedimentary basins. *Proceedings of the 8th Conference on Greenhouse Gas Technologies*.

Class, H. et al. [2009] A benchmark study on problems related to CO2 storage in geologic formations. *Comp. Geosci.*, **13**(4), 409–434, doi:10.1007/s10596-009-9146-x.

Coats, K.H., Dempsey, J.R. and Henderson, J.H. [1971] The use of vertical equilibrium in two-dimensional simulation of three-dimensional reservoir preformance. *Soc. Pet. Eng. J.*, **Mar**, 68–71.

Coats, K.H., Nielsen, R.L., Terune, M.H. and G.Weber, A. [1967] Simulation of three-dimensional, two-phase flow in oil and gas reservoirs. *Soc. Pet. Eng. J.*, **Dec**, 377–388.

Hesse, M.A., Orr, F.M. and Tchelepi, H.A. [2008] Gravity currents with residual trapping. *J. Fluid. Mech.*, **611**, 35–60.

Hesse, M.A., Tchelepi, H.A., Cantwell, B.J. and Orr, F.M. [2007] Gravity currents in horizontal porous layers: transition from early to late self-similarity. *J. Fluid. Mech.*, **577**, 363–383.

Holden, H., Karlsen, K.H., Lie, K.A. and Risebro, N.H. [2010] *Splitting Methods for partial Differential Equations with Rough Solutions: Analysis and* MATLAB *programs*, vol. 11 of *EMS Series of Lectures in Mathematics*. European Mathematical Society.

Holden, H. and Risebro, N.H. [2002] *Front Tracking for Hyperbolic Conservation Laws*, vol. 152 of *Applied Mathematical Sciences*. Springer-Verlag, New York, ISBN 3-540-43289-2.

Huppert, H.E. and Woods, A.E. [1995] Gravity-driven flows in porous layers. *J. Fluid Mech.*, **292**, 55–69.

Kružkov, S.N. [1970] First order quasilinear equations in several independent variables. *Math USSR Sbornik*, **10**(2), 217–243.

Lyle, S., Huppert, H.E., Hallworth, M., Bickle, M. and Chadwick, A. [2005] Axisymmetric gravity currents in a porous media. *J. Fluid. Mech.*, **543**, 293–302, doi:10.1017/S0022112005006713.

MacMinn, C.W. and Juanes, R. [2009] Post-injection spreading and trapping of CO_2 in saline aquifers: Impact of the plume shape at the end of injection. *Comp. Geosci.*, **13**, 483–491.

Martin, J.C. [1958] Some mathematical aspects of two phase flow with application to flooding and gravity segregation. *Prod. Monthly*, **22**(6), 22–35.

Martin, J.C. [1968] Partial integration of equation of multiphase flow. *Soc. Pet. Eng. J.*, **Dec**, 370–380.

Mishara, S. and Jaffré, J. [2010] On the upstream mobility scheme for two-phase flow in porous media. *Comput. Geosci.*, **14**(1), 105–124.

Nordbotten, J.M. and Celia, M.A. [2006] Analysis of plume extent using analytical solutions for CO_2 storage. *Proceedings of the 16th conference on Computational Methods in Water Resources*.

Nordbotten, J.M. and Celia, M.A. [2010] *Geological Storage of CO_2: Modeling Approaches for Large-Scale Simulation*. In preparation.

Nordbotten, J., Celia, M. and Bachu, S. [2005] Analytical solution for CO2 plume evolution during injection. *Transp. Porous Media*, **58**(3), 339–360.

Ruben Juanes, C.W.M. and Szulczewski, M.L. [2010] The footprint of the CO2 plume during carbon dioxide storage in saline aquifers: Storage efficiency for capillary trapping at the basin scale. *Transp. Porous Media*, **82**(1), 19–30, doi:10.1007/s11242-009-9420-3.

Vella, D. and Huppert, H.E. [1995] Gravity currents in a pourous medium at an inclinded plane. *Journal of Fluid Mechanics*, **292**, 59–65.